New Algorithm for Optimised Fitting of DIC Data to Crack Tip Plastic Zone Using the CJP Model

Bing Yang[a], Zhanjiang Wei[a], F A Díaz[b], Zhen Liao[a] and M N James[c, d]

[a] State Key Laboratory of Traction Power, Southwest Jiaotong University, Chengdu, China

[b] Departamento de Ingeniería Mecánica y Minera, Universidad de Jaén, Jaén, Spain

[c] School of Engineering, University of Plymouth, Plymouth, England, United Kingdom

[d] Department of Mechanical Engineering, Nelson Mandela Metropolitan University, Port Elizabeth, South Africa

Abstract: The work presented in this paper provides guidance in optimally determining the appropriate fitting region used in digital image correlation (DIC) when fitting a crack tip field model to DIC data.   In this work, the technique is applied to the CJP crack tip field model and uses the Levenberg-Marguardt (L-M) iterative method to solve for the crack tip position. This is combined with an error analysis of the main term of the Williams series expansion for crack tip stresses and the extrapolation of Saint-Venant's principle to determine the optimum fitting region for use in DIC fit with the multi-parameter solution for the CJP crack tip field model. A comparison is then made between the size and shape of the crack tip plastic zone obtained using the Williams and the CJP models. This demonstrated that as the plastic zone size increased, there was a deterioration in accuracy of the description of the crack tip plastic zone using the Williams series expansion, while the CJP description remains more accurate. In addition, K_F, the stress-intensity factor that drives crack growth in the CJP model has a strong linear relationship with the plastic zone area, which indicates that K_F is a direct driving force for crack growth and there is a clear relationship between ΔK_{CJP} and ΔK_{I}.

Keywords: Crack tip fields, CJP model, Digital image optimisation, Levenberg-Marguardt iterative method, Plasticity-induced shielding

1 Introduction

In early studies of fatigue crack growth of structures, it was considered that crack wake contact (closure) could only occur under the action of compressive loading. When Rice [1] studied the stress field at a crack tip, he excluded the possibility of crack closure under cyclic loading. However, Elber [2] in work on centre-cracked tension specimens, observed that this would be true only for an idealised crack that is not

propagating, and proposed that partial crack closure would occur after unloading due to the permanent tensile deformation left in the wake of the crack. His work on centre-cracked tension specimens led him to propose the concept of crack closure. The crack closure effect on fatigue crack growth has been widely accepted with the crack opening level proposed to have a significant effect on fatigue crack growth rate [3]. Many papers have been published on crack closure measurement techniques and on models that have been proposed to determine the effect of crack closure on the crack growth rate [e.g. 3-7]. It is widely accepted that when a crack tip plastic zone occurs under an applied tensile stress, residual stresses can lead to crack surface contact (closure) during unloading. For instance, Beevers et al [8] proposed a 2-dimensional model based on a single asperity contact under Mode I plane strain conditions where contact produces a compression of the asperity during the lower portion of the load cycle. However, definitive measurements of the stress arising from contact between the upper and lower fracture surfaces in the crack tip region have never been reported and measurements of closure are usually either indirect, e.g. compliance-based, or inferred from visual examination.

Indirect measurement methods have placed a limit on understanding the physical basis of fatigue crack closure mechanisms [9]. Full field experimental techniques have recently become widely available and provide an opportunity to revisit mechanistic understanding of fatigue crack closure. They can provide full field displacement or stress data that can then be fitted to advanced crack tip field models that better capture the effects of a crack tip plastic zone on the local displacement or stress field, and can therefore offer insights into the physical mechanisms of closure. Polycarbonate is a refractive, ductile material whose fatigue properties have been widely studied. It is suitable for investigation with the photoelastic method, where isochromatic fringes are used to establish a direct functional relationship with the stress field; thus, this method is accurate and potentially able to resolve wake contact forces.

Polycarbonate was employed by Pacey at al [10] in photoelastic work on 2 mm thick compact tension specimens, that was aimed at elucidating the crack wake contact force in fatigue crack closure. That work used the Muskhelishvili complex potential method to obtain a mathematical model to describe the stresses near the tip of a crack that is experiencing a single-point fracture surface contact. This model was fitted to the full-field experimental data measured by photoelasticity near the crack tip [10], using a combination of a simple genetic algorithm and the downhill simplex optimisation method to perform the fitting quickly and accurately. Stress intensity factors measured during two load cycles fitted well with the applied load

cycle and clearly displayed evidence of plasticity-induced shielding on the effective stress intensity factor. However, the results given by the model showed that the pressure exerted on the crack flanks was random, and did not follow a consistent trend with the applied load cycle.

This led the authors to consider what additional plasticity-induced stresses might be affecting crack tip shielding and, in 2007, Christopher et al [11] proposed a new model for the crack tip stress field that included additional force terms to describe an exponential distribution of wake contact behind the crack tip and a compatibility-induced stress acting along the crack plane at the notional elastic-plastic boundary. This mathematical model was referred to as the Christopher-James-Patterson (CJP) model. Initially, this model was applied to the same polycarbonate compact tension (CT) specimens as had been used for the previous work reported by Pacey et al [10], and the results demonstrated that the CJP model accurately described the effective driving force for fatigue crack growth in polycarbonate in the presence of plasticity-induced shielding. In order to extend the work to metallic alloys, a displacement-based solution for the CJP model was reported by James et al [12] and this allowed the digital image correlation technique to be used and fitted to the CJP model on a full-field basis. Vasco-Olmo et al [13] used the DIC technique in combination with the CJP model to obtain the crack tip plastic zone size and shape, both via the model and experimentally, and compared the CJP model predictions with those provided by the Williams and Westergaard crack tip stress models. The results showed that the CJP model gave size and shape data that was the closest to the experimentally measured values.

However, in applying the DIC technique to the measurement of crack tip fields, the position of the crack tip is an important parameter that affects the accuracy of the results obtained for the stress parameters in the CJP model. James et al [12] highlighted the sensitivity of the results obtained from the CJP model to selection of the region used to fit the experimental displacement or stress field. They used an empirical exploration of the influence of the data collection region and the crack tip position to identify optimum values for these parameters. A number of different optimisation techniques have been used in other published work that has used DIC techniques to characterise the crack tip displacement field so as to calculate a stress intensity factor. These include Newton-Raphson iteration, the use of genetic algorithms, the simplex method, and the pattern search technique [14-18]. However, the use of mathematical methods to determine the optimal crack tip position when using the CJP model has not been reported in detail yet.

In summary, although the crack closure effect has been widely studied, improved crack tip field

models are required to advance understanding of the mechanisms involved and to be able to better predict the influence of loading parameters, such as mean cyclic stress and variable amplitude loading, on crack tip shielding and hence on crack growth rates. Only then can an improved predictive capability be developed for fatigue crack growth rate and fatigue life prediction. The CJP model is a more complete mathematical model of the elastic crack tip stress field in the presence of plasticity-induced shielding and represents an advance over the Williams or Westergaard models. Reference [19] has shown that although the CJP model, like the Westergaard model and the Williams model, uses coordinate axes aligned with the crack tip, the CJP model leads to stress intensity factors that are geometry-independent, at least for CT and double edge-notched tension specimens. Hence there is no necessity for a compliance-based geometry correction factor. The more inclusive physical basis of the model also provides a wider range rationalisation of crack growth rate data as a function of stress ratio and effective range of stress intensity factor than is possible using the Paris relationship for crack growth rate.

However, a significant issue in applying the CJP model to digital image correlation relates to an optimum identification of the crack tip position, which is hard to accurately measure and position in the measured crack tip displacement field, while the selection of an optimum fitting region in terms, typically, of inner and outer measurement radii can only be assessed experimentally, which is time-consuming and potentially inaccurate.

To address these problems, this study proposes the use of the Levenberg-Marguardt (L-M) iterative method to solve for the crack tip position based on the CJP model. Then, combined with the error analysis of the main term of the Williams series and the generalization of the Saint-Venant principle, a more theoretically-based method for selecting the fitting area is developed. An analysis of the actual displacement field shows that the proposed methods for determining the crack tip position and selecting the fitting area are effective. The work presented in this paper can therefore provide guidance in an optimised application of the CJP model (or other crack tip field model) to full-field experimental displacement data obtained via digital image correlation.

2 Introduction to CJP model

2.1 Williams model

The Williams model is based on linear elastic fracture mechanics and uses the mathematical form of an infinite series to describe the crack tip stress field distribution in a stable state, drawing from previous research results [20]. According to this model the crack tip stress field for a mode I crack can be expressed as a function of the number of adopted terms in the series, the series coefficients and the polar coordinates of a set of points at the region surrounding the crack tip[13]:

$$\sigma_x = \sum_{n=1}^{\infty} \frac{n}{2} A_n r^{\frac{n-2}{2}} \left\{ \left[2 + (-1)^n + \frac{n}{2} \right] \cos\left(\frac{n}{2} - 1\right)\theta - \left(\frac{n}{2} - 1\right)\cos\left(\frac{n}{2} - 3\right)\theta \right\} \quad (1a)$$

$$\sigma_y = \sum_{n=1}^{\infty} \frac{n}{2} A_n r^{\frac{n-2}{2}} \left\{ \left[2 - (-1)^n - \frac{n}{2} \right] \cos\left(\frac{n}{2} - 1\right)\theta - \left(\frac{n}{2} - 1\right)\cos\left(\frac{n}{2} - 3\right)\theta \right\} \quad (1b)$$

$$\sigma_{xy} = \sum_{n=1}^{\infty} \frac{n}{2} A_n r^{\frac{n-2}{2}} \left\{ -\left[(-1)^n + \frac{n}{2} \right] \sin\left(\frac{n}{2} - 1\right)\theta - \left(\frac{n}{2} - 1\right)\sin\left(\frac{n}{2} - 3\right)\theta \right\} \quad (1c)$$

Where $A_1 = K_I/\sqrt{2\pi}$ and $A_2 = -T/4$.

Close to the crack tip ($r/a \ll 1$), the first two terms in the series, which are equivalent to the Westergaard function expression [12], are sufficient to characterise the stress field in this area. In a similar way, the displacement fields around the crack tip can be described as[13]:

$$u = \sum_{n=1}^{\infty} \frac{r^{n/2}}{2G} a_n \left\{ \left[\kappa + \frac{n}{2} + (-1)^n \right] \cos\frac{n\theta}{2} - \frac{n}{2}\cos\frac{(n-4)\theta}{2} \right\}$$

$$(2a)$$

$$v = \sum_{n=1}^{\infty} \frac{r^{n/2}}{2G} a_n \left\{ \left[\kappa - \frac{n}{2} - (-1)^n \right] \sin\frac{n\theta}{2} + \frac{n}{2}\sin\frac{(n-4)\theta}{2} \right\} \quad (2b)$$

Where $a_1 = K_I/\sqrt{2\pi}$ $a_2 = T/4$, G is the shear modulus, E and υ are the Young's modulus and the Poisson's ratio of the material respectively and, $\kappa = (3-\upsilon)/(1+\upsilon)$ for plane stress or $\kappa = 3 - 4\upsilon$ for plane strain.

2.2 CJP crack tip field model

Fatigue of ductile materials occurs via plastic deformation processes at the crack tip, and the Poisson's ratio in the plastic region is different from that in the elastic region (plastic deformation is a constant volume process with $v = 0.5$), which necessarily produces a compatibility stress at the elastic–plastic boundary. Moreover, contact of the crack surfaces during crack propagation induces an additional stress distribution near the tip. Both of the compatibility and contact stresses will have an effect on the applied stress field ahead of the crack, and are not considered in the Williams crack tip stress expansion series. Both of these stresses are the result of plasticity-induced shielding. CJP model is based on Muskhelishvili's complex potentials [21], and it postulates that the plastic enclave that exists around a fatigue crack tip and along the crack flanks will shield the crack from the full influence of the applied elastic stress field. According to this, the crack tip stress field equations are then described by the following expressions [12]:

$$\sigma_x = -\frac{1}{2}(A+4B+8E)r^{-\frac{1}{2}}\cos\frac{\theta}{2} - \frac{1}{2}Br^{-\frac{1}{2}}\cos\frac{5\theta}{2} - C - \frac{1}{2}Er^{-\frac{1}{2}}\left[\ln(r)\left(\cos\frac{5\theta}{2}+3\cos\frac{\theta}{2}\right)+\theta\left(\sin\frac{5\theta}{2}+3\sin\frac{\theta}{2}\right)\right] \tag{3a}$$

$$\sigma_y = \frac{1}{2}(A-4B-8E)r^{-\frac{1}{2}}\cos\frac{\theta}{2} + \frac{1}{2}Br^{-\frac{1}{2}}\cos\frac{5\theta}{2} + \frac{1}{2}E^{-\frac{1}{2}}\left[\ln(r)\left(\cos\frac{5\theta}{2}-5\cos\frac{\theta}{2}\right)+\theta\left(\sin\frac{5\theta}{2}-5\sin\frac{\theta}{2}\right)\right] \tag{3b}$$

$$\sigma_{xy} = -\frac{1}{2}r^{-\frac{1}{2}}\left(A\sin\frac{\theta}{2}+B\sin\frac{5\theta}{2}\right) - Er^{-\frac{1}{2}}\sin\theta\left[\ln(r)\cos\frac{3\theta}{2}+\theta\sin\frac{3\theta}{2}\right] \tag{3c}$$

Where $A+B \neq 0$, $D+E=0$, $C=-T$.

Unlike the Williams model, the CJP model leads to three stress-intensity factors [12, 13, 19]: K_F, the stress-intensity factor that drives the crack forwards and reduces to the standard Irwin stress-intensity factor if no plasticity is present; K_R, a stress intensity-factor that retards crack propagation and arises from the action of crack wake contact and the compatibility-induced stresses; and K_S, a shear stress-intensity factor generated by the compatibility-induced stresses at the elastoplastic boundary. The three stress-intensity factors are expressed as follows:

$$K_F = \lim_{r \to 0} \left[\sqrt{2\pi r} \left(\sigma_y + 2Er^{-1/2} \ln r \right) \right] = \sqrt{\frac{\pi}{2}} \left(A - 3B - 8E \right) \tag{4a}$$

$$K_R = \lim_{r \to 0} \left[\sqrt{2\pi r} \sigma_x \right] = -\left(2\pi \right)^{1.5} E \tag{4b}$$

$$K_S = \lim_{r \to 0} \left[\sqrt{2\pi r} \sigma_{xy} \right] = \pm \sqrt{\frac{\pi}{2}} \left(A + B \right) \tag{4c}$$

To use DIC technology with the CJP model to study fatigue crack growth rate in metallic alloys, the following complex variable function of the displacement field of the model must be used [12]:

$$
\begin{aligned}
2G(u + iv) = \kappa &\left[-2Bz^{0.5} - 2Ez^{0.5} \ln(z) - \frac{C}{4} z \right] - \\
z &\left[-(B + 2E)\overline{z}^{-0.5} - E\overline{z}^{-0.5} \overline{\ln(z)} - \frac{C}{4} \right] - \\
&\left[A\overline{z}^{-0.5} + D\overline{z}^{-0.5} \overline{\ln(z)} + 2D\overline{z}^{-0.5} + \frac{C}{2} \overline{z} \right]
\end{aligned}
\tag{5}
$$

Where $\kappa = (3 - \upsilon)/(1 + \upsilon)$ is the plane stress state; $\kappa = 3 - 4\upsilon$ is the plane strain state; and υ is Poisson's ratio of the material in the elastic region. It should be noted that under Mode I or Mode I plus II loading, it appears that K_F and K_R provide sufficient information to characterize the effective driving force for crack growth. It is believed that under Mode III loading, K_S will prove to have utility. It should also be noted that, from the way in the which the force components were defined in the CJP model, negative values of K_R have significance.

3 Solving for the CJP model stress parameters

3.1 Linear fitting

As mentioned above, accurate determination of the position of the crack tip is an important prerequisite in using DIC techniques to obtain the parameters in crack tip field models such as the CJP model. In previous work, the discontinuous characteristics of the vertical displacement field at the crack tip have generally been used to determine the position of the crack tip [19, 22] . If the coordinates of the crack tip position are known, the CJP model parameters can be found using a linear fitting method. Assuming that the discontinuous characteristics of the displacement field are used to obtain the coordinates of the crack

tip (x_o, y_o), $z = (x - x_o) + i(y - y_o)$, the real and imaginary parts of the stress field equation (5) can be separated. Substituting $D = -E$ into equation (5) then gives:

$$2G(u + iv) = Af_1(z) + Bf_2(z) + Cf_3(z) + Ef_4(z) \tag{6a}$$

$$f_1(z) = -z^{-0.5}$$
$$h_1 = \text{Re}(f_1), g_1 = \text{Im}(f_1) \tag{6b}$$

$$f_2(z) = -2\kappa z^{0.5} + z\bar{z}^{-0.5}$$
$$h_2 = \text{Re}(f_2), g_2 = \text{Im}(f_2) \tag{6c}$$

$$f_3(z) = -\frac{1}{4}\kappa z + \frac{1}{4}z - \frac{1}{2}\bar{z}$$
$$h_3 = \text{Re}(f_3), g_3 = \text{Im}(f_3) \tag{6d}$$

$$f_4(z) = -(2\kappa z^{0.5}\ln(z) - 2z\bar{z}^{-0.5} - z\bar{z}^{-0.5} - z^{-0.5}\overline{\ln(z)} + 2\bar{z}^{-0.5})$$
$$h_4 = \text{Re}(f_4), g_4 = \text{Im}(f_4) \tag{6e}$$

The measured displacement fields contain both translation and rotational components, as if the specimen rotates slightly with point P as the center of rotation ($R<<1$), then the displacement of point P represents both the deformation and a rigid body translation, which can be written as shown in equation (7):

$$u = \frac{1}{2G}(Ah_1 + Bh_2 + Ch_3 + Eh_4) + u'_x$$
$$v = \frac{1}{2G}(Ag_1 + Bg_2 + Cg_3 + Eg_4) + u'_y \tag{7}$$

In this equation, u'_x and u'_y are the translational components of the sample. The position of the crack tip can be used as the coordinate origin to establish a rectangular coordinate system. Assuming that the coordinates of the rotation center point P are (x_p, y_p), as shown in Fig. 1, the coordinates of any point A in the coordinate system are (x, y), the rotation of the sample causes point A to move to A', and the motion component is given by equation (8):

$$u' = RL\cos\beta$$
$$v' = RL\sin\beta \tag{8}$$

Where $L = \sqrt{(x - x_p)^2 + (y - y_p)^2}$

The Pythagoras relationship between the sides of a triangle can be used to obtain equation (9):

$$u` = Ry - Ry_p$$
$$v` = Rx - Rx_p$$
(9)

Therefore, when the crack tip is taken as the origin of the coordinates, the total displacement equation of any point A is:

$$u = \frac{1}{2G}\left(Ah_1 + Bh_2 + Ch_3 + Eh_4\right) + u_x - Ry$$
$$v = \frac{1}{2G}\left(Ag_1 + Bg_2 + Cg_3 + Eg_4\right) + u_y + Rx$$
(10)

Where

$$u_x = u`_x + Ry_p$$
$$v_y = u`_y - Rx_p$$
(11)

Selecting a region near the crack tip for the fitting process gives the inverse equation system as $KX = b$, with the matrix form as shown in equation (12):

$$K = \begin{pmatrix} h_{11} & h_{12} & h_{13} & h_{14} & 1 & 0 & -y_1 \\ h_{21} & h_{22} & h_{23} & h_{24} & 1 & 0 & -y_2 \\ M & M & M & M & M & M & M \\ h_{n1} & h_{b2} & h_{n3} & h_{n4} & 1 & 0 & -y_n \\ g_{11} & g_{12} & g_{13} & g_{14} & 0 & 1 & x_1 \\ g_{21} & g_{22} & g_{23} & g_{24} & 0 & 1 & x_2 \\ M & M & M & M & M & M & M \\ g_{n1} & g_{n2} & g_{n3} & g_{n4} & 0 & 1 & x_n \end{pmatrix}$$
(12)

$$X = \left(A, B, C, E, u_x, u_y, R\right)^T$$
(13)

$$b = \left(u_1, u_2, \text{L}, u_m, v_1, v_2, \text{L}, v_m\right)^T$$
(14)

The solution of the inverse system of equations is given by $X = \left(K^T K\right)^{-1}\left(K^T b\right)$, from which the parameters in the CJP model can be determined.

3.2 Nonlinear fitting method

3.2.1 Solving nonlinear equations

The mathematical calculation of the stress parameters in the CJP model using the linear fitting method is not complicated. However, due to the bluntness of the crack tip, the actual displacement field does not

have the theoretically expected form near the crack tip. It is also difficult to find the location of the crack tip accurately from the discontinuity of the vertical displacement field and precise location of the crack tip is very important in determining accurate parameter values [13]. To solve this problem, the crack tip position can be used as an unknown quantity and calculated along with other parameters using a nonlinear iteration method. The real functions of the pure Mode I crack displacement field are expressed as follows [23]:

$$
\begin{aligned}
2Gu = {} & r^{0.5}\left(-A-2B\kappa-2E\right)\cos\frac{\theta}{2}+r^{0.5}\left(B+2E\right)\cos\frac{\theta}{2}- \\
& r^{0.5}E\left[\ln(r)\left(\cos\frac{3\theta}{2}+(1-2\kappa)\cos\frac{\theta}{2}\right)+\theta\left(\sin\frac{3\theta}{2}+(2\kappa-1)\sin\frac{\theta}{2}\right)\right]- \\
& \frac{C}{4}r(1+\kappa)\cos\theta
\end{aligned} \tag{15a}
$$

$$
\begin{aligned}
2Gv = {} & r^{0.5}\left(A-2B\kappa-2E\right)\cos\frac{\theta}{2}+r^{0.5}\left(B+2E\right)\cos\frac{\theta}{2}+ \\
& r^{0.5}E\left[\ln(r)\left(\sin\frac{3\theta}{2}-(1+2\kappa)\sin\frac{\theta}{2}\right)-\theta\left(\cos\frac{3\theta}{2}+(1+2\kappa)\cos\frac{\theta}{2}\right)\right]+ \\
& \frac{C}{4}r(3-\kappa)\sin\theta
\end{aligned} \tag{15b}
$$

where $r=\sqrt{\left(x_i-x_o\right)^2+\left(y_i-y_o\right)^2}$, $\theta=\mathrm{acos}\left(\left(x_i-x_o\right)/r\right)$, and $\left(x_o,y_o\right)$ are the crack tip coordinates. Assuming that the unknown quantity is $Z=\left(A,B,C,E,x_o,y_o,u_x,u_y,R\right)$, we can write an objective function expression as (16):

$$
F(Z)=\sum_{i=1}^{m}\left(\left[u_i(x_i,y_i;Z)-U_i\right]^2+\left[v_i(x_i,y_i;Z)-V_i\right]^2\right) \tag{16}
$$

The solution $F(Z)$ that minimises the objective function Z is the optimal solution, and U_i,V_i are the horizontal and vertical displacements corresponding to the point $\left(x_i,y_i\right)$ measured using the DIC technique. The Gauss-Newton (G-N) iterative algorithm or the modified Levenberg-Marguardt (L-M) iterative algorithm can be used to the calculate numerical solutions. Because the latter is more suitable for the nonlinear solution of the ill-conditioned matrix in the iterative process, the numerical solution of the L-M iterative algorithm was used in this study. In concise form, we assume $p_i=u_i(x_i,y_i;Z)-U_i$, $q_i=v_i(x_i,y_i;Z)-V_i$:

$$F(Z) = \sum_{i=1}^{m} \left(p_i^2 + q_i^2 \right) \tag{17}$$

The iteration format of the L-M algorithm is [24]:

$$\Delta Z_k = -\left[DF(Z_k)^T DF(Z_k) + \mu_k I \right]^{-1} DF(Z_k)^T F(Z_k)$$
$$Z_{k+1} = Z_k + \Delta Z_k \tag{18}$$

$DF(Z)$ is a Jacobi matrix, which can be obtained from the derivation rule as follows:

$$DF(Z) = \begin{pmatrix} \dfrac{\partial u_1}{\partial z_1} & \dfrac{\partial u_2}{\partial z_1} & \mathrm{L} & \dfrac{\partial u_m}{\partial z_1} \dfrac{\partial v_1}{\partial z_1} & \dfrac{\partial v_2}{\partial z_1} & \mathrm{L} & \dfrac{\partial v_m}{\partial z_1} \\[2mm] \dfrac{\partial u_1}{\partial z_2} & \dfrac{\partial u_2}{\partial z_2} & \mathrm{L} & \dfrac{\partial u_m}{\partial z_2} \dfrac{\partial v_1}{\partial z_2} & \dfrac{\partial v_2}{\partial z_2} & \mathrm{L} & \dfrac{\partial v_m}{\partial z_2} \\[2mm] \mathrm{M} & \mathrm{M} & \mathrm{L} & \mathrm{M} \quad \mathrm{M} & \mathrm{M} & \mathrm{L} & \mathrm{M} \\[2mm] \dfrac{\partial u_1}{\partial z_9} & \dfrac{\partial u_2}{\partial z_9} & \mathrm{L} & \dfrac{\partial u_m}{\partial z_9} \dfrac{\partial v_1}{\partial z_9} & \dfrac{\partial v_2}{\partial z_9} & \mathrm{L} & \dfrac{\partial v_m}{\partial z_9} \end{pmatrix}^{T} \tag{19}$$

where $\left(\partial u_i / \partial z_j \right) = \left(\partial u / \partial z_j \right)\big|_{\substack{x=x_i \\ y=y_i}}$; $\left(\partial v_i / \partial z_j \right) = \left(\partial v / \partial z_j \right)\big|_{\substack{x=x_i \\ y=y_i}}$; $z_i, (i=1,2\mathrm{L}\ 9)$ represents each un-

known parameter in Z; and $\zeta = \sqrt{\sum_{i=1}^{m} \left[\left(p_i / U_i \right)^2 + \left(q_i / V_i \right)^2 \right]}$ is the 2-norm of the relative error of the fitted

area. In the G-N iterative method, the iterative matrix is $DF(Z_k)^T DF(Z_k)$. In the L-M algorithm, μ_k is

added as a damping factor to change the iterative matrix to $DF(Z_k)^T DF(Z_k) + \mu_k I$. The introduction of

μ_k can help improve the condition number of the iterative matrix $DF(Z_k)^T DF(Z_k)$, but as μ_k in-

creases, the convergence speed of the iterative method will slow down. Changing μ_k during the iterative

process ensures that the iterative matrix is always in a non-ill-conditioned state, which improves the solu-

tion accuracy. Changing μ_k can make each effective iteration converge toward a decreasing objective

function, ensuring that the final solution is as close as possible to the global optimal solution. Wang [24]

proposed several methods for updating the damping factors during the iterative process. The goal is to both

improve the ill-conditioned characteristics of the iterative matrix and converge the iteration toward reduc-

ing the objective function; this complicates the iterative process considerably. The ill-conditioned equation

can be solved using the pre-processing conjugate gradient (PCG) algorithm to ensure that the solution is

accurate. Therefore, the selection of the damping factor μ_k in the iteration process only needs to ensure that the iteration converges towards reducing the objective function. At the beginning of the iteration, a small μ_0 can be selected to accelerate the convergence of the initial iteration and in this work was selected with a value between 10^{-7} and 10^{-5}. It should be noted that this value maybe not suitable in all cases. Research is currently ongoing to determine whether a suitable generalised value of μ_0 can be determined.

3.2.2 Choosing the fitting area

Another factor that affects the accuracy of determination of the parameters in the CJP model is the selection of the fitting area during the iteration process. Usually, an over-deterministic approach is adopted where measurement points are placed evenly along a series of concentric arcs around the crack tip. As the CJP model is an improved elastic model that accounts for plasticity through its effects on the elastic field ahead of the crack tip, the measurement region has to exclude the crack tip plastic zone. The inner radius of these arcs can therefore be related to the size of the crack tip plastic zone, which can be obtained by processing the displacement field data using the material parameters. The detailed method for calculating the plastic zone is described in section 4.2.

The determination of the outer radius is more complicated because the CJP model represents the effects of an applied Mode I stress and two additional terms representing the stresses induced by the plastic enclave around the crack. The stress field region where the CJP model is valid should be similar to that where the first term in the Williams stress expansion is capable of characterising the actual crack stress field. Zhou et al [25] theoretically derived the solution accuracy of the first term in the Williams series. The calculation results showed that for a crack with a half-length of 1 cm and considering a circular region around the crack tip with radii r = 1 mm and 2 mm, the maximum truncation error between the Williams approximate stress solution and the exact solution are 6.8% and 12.6%, respectively.

Following on from this, a general rule of thumb is that a stress intensity approach based on the first term in the Williams series expansion requires that the plastic zone should not exceed 1/20 of the crack length and the first term approximation is only valid outside this region. However, in many practical situations, this range does not give conservative results and the calculated stress intensity factor will be underestimated due to plastic blunting of the crack tip. With respect to the calculation results presented herein,

the outer radius of the fitting area should not also exceed 1/5 of the crack length. As the CJP model considers a compatibility stress at the elastic-plastic boundary and a stress arising from contact between crack surfaces, the generalized Saint-Venant's principle [26] shows that the action range of these two stresses should be only 1–2 times the maximum radius of the plastic zone. It is therefore fairly usual to consider an outer radius as 1/10 of the crack length. A suitable fitting area for the DIC data and the CJP crack tip field model hence has an inner radius related to the plastic zone size and an outer radius related to the crack length. Optimum values can therefore be determined through an iterative process.

3.2.3 Algorithm introduction

The initial value chosen in the nonlinear iteration is important, as it affects the convergence and the solution found. In the present study a reasonable initial value for the iteration was obtained by first estimating the crack tip position, and then using linear to solve for the other parameters. These parameters together form a set of initial values for the non-linear iteration. An appropriate initial value can greatly reduce the number of nonlinear iterations.

A reasonable convergence criterion to terminate the iteration is necessary for the non-linear iteration. After every step of iteration, the displacement field corresponding to the current theoretical solution is found. The theoretical displacement field is then compared with the experimental field, and the 2-norm of the relative error (ζ) is taken as the convergence criterion. This convergence criterion ensures that the theoretical displacement field obtained through the fitting process is in good agreement with the experimental displacement field. In the present study, the iterative process is terminated when $\zeta < \varepsilon = 0.05$. It is worth noting that $\varepsilon = 0.05$ may not satisfy all other cases, but it was effective in this research, reducing the number of iterations to the range 4 - 6, and the total time to between 80 s and 120 s.

The specific steps of the nonlinear iterative algorithm are shown in flowchart 1.

4 Experimental Verification

4.1 Experiment

Experimental verification of the iterative process developed in this paper used U71MnG rail steel with the mechanical properties shown in Table 1. A double edge-notched tension (DENT) specimen was used

with dimensions shown in Fig. 2. One surface of the DENT specimen used for the DIC analysis was sprayed with a random black speckle pattern over a white background, and the other surface of the specimen was ground and polished to allow tracking of the crack tip position with a precision of 10 μm. A charge-couple device camera equipped with a macro-zoom lens (MLH-10X EO) was vertically aligned on the speckled surface of the specimen, with a field of view of approximately 19 mm × 14 mm and a resolution of 11.7 μm/pixel. Fatigue crack growth rate testing was performed using sinusoidal loading cycles on an Electro-Puls E3000 dynamic testing machine with maximum load of 2400 N and a stress ratio of 0.1 at 10 Hz. In the DIC work, the facet size was 45 pixel and each facet overlapped by 11 pixel.

Table 1 Mechanical performance parameters of test material

$E(\%)$	$\sigma_b(\text{MPa})$	$\sigma_s(\text{MPa})$	$\varepsilon_f(\%)$	υ
210,000	≥ 880	780	≥ 10	0.28

4.2 Algorithm application

The following process was employed to verify that the optimization of the crack tip position did indeed give better results than obtained without the optimization process. The two different crack tip positions (estimated and optimised) were used to calculate the corresponding CJP model parameters. These parameters were then used to solve for the theoretical displacement field being characterised by the CJP model. Finally, the mean value and variance were determined in the relative error between the two theoretically obtained displacement fields and that measured experimentally. For example, Table 2 shows the tip coordinates obtained using the two methods and the corresponding mean value and variance in the relative error for the case when the crack length was 18.27 mm and the load was 2400 N. It can be seen that the values obtained using the proposed method are significantly smaller than those calculated using the conventional method.

Table 2 The mean value and the variance of the relative error of the displacement field using two different methods

Parameter	Conventional method	Proposed method
Tip coordinates (pixel)	(820, 660)	(809.5, 647.8)
Mean $E(\eta)$	2.532×10^{-6}	-6.954×10^{-7}
Variance $D(\eta)$	1.283×10^{-5}	1.340×10^{-6}

In this work, the plastic zone size has been used as a comparative parameter of optimisation success because it is well-recognised as a controlling parameter in fatigue crack growth rate. Suzuki and McEvily [27], amongst others, showed that the size of the crack tip plastic zone was related to the crack growth rate and the crack tip plastic zone produces the crack wake, which in turn causes plastic-induced shielding [2]. It is therefore meaningful to study the advantages of the CJP model in describing the plastic zone size (and shape).

Obtaining an accurate experimental size for the crack tip plastic zone is an important prerequisite when studying the advantages of the CJP model in characterizing the plastic zone. In this process, the most important step is solving for the strain from the displacement field. Pan et al [28] proposed a local least-squares fitting method based on the full-field displacement, which has been shown to be a useful algorithm for solving for strain. Subsequently, the stress field can be obtained using the generalised form of Hooke's law combining the physical equation of elastic mechanics, and the size of the experimental plastic zone obtained by substituting the von Mises or Tresca yield criteria [29]. In the present study, the von Mises criterion was used.

Comparing the theoretically obtained CJP plastic zone with the experimental determined plastic zone both before and after optimization, as shown in Fig. 3, shows that the optimized plastic zone is significantly smaller than the one obtained before optimization, and is also closer to the experimental plastic zone.

It should be noticed that the shape of this plastic zone is irregular because the displacement field measured by DIC is a set of discrete points. In present study, a rectangular region with length l and width w is used in the DIC measurements. If there are m measurement points located in this rectangular field in total and n measurement points located in the plastic zone around the crack tip, then the experimental area of the plastic zone, A_e, can be determined by calculating $A_e = l \times w \times n/m$. Though the analysis results could show the effectiveness of present method for calculating the area of the plastic zone, an improved technique is being developed to further reduce the fitting error. When comparing the plastic zone predictions given by two different models, such as the Williams and CJP models, the chosen fitting areas for both models should be the same. As explained in the previous section, the outer radius of the fitting area is selected as $r \le 0.1a$, with a being the crack length of the sample.

The plastic zone shape and area estimated using the CJP model, and using the Williams model with the first term, 3-terms and 5-terms have been calculated and are listed in Table 3. To determine whether the

CJP model or the Williams model describes the plastic zone more effectively, it is advantageous to use a relatively long crack length where the crack tip plastic zone is large enough to emphasize differences. The relative error between each of these predicted plastic zone areas, A_p, and the experimentally determined one is defined as $e=(A_p-A_e)/A_e$, which is also given in Table 3. Data was acquired at crack lengths L = 17.26, 17.65, 18.27, and 18.67 mm under the maximum load of P = 2400 N, as depicted in Figures 4a through 4d.

These figures clearly show that the difference between the predicted plastic zone and the experimentally measured plastic zone for each of the models. At all crack lengths considered, the CJP model provides the closest estimate with relative errors, e, ranging from -1.52% at a crack length of 17.26 mm to +5.98% at 18.77 mm. In contrast, errors for the first term approximation of the Williams model ranges from +1.96% (17.26 mm) to +24.98% (18.27 mm). These relative errors decrease again for both the CJP and Williams models at a crack length of 18.67 mm. Using a three or five term Williams approximation decreases the accuracy of the fit at the three smaller crack lengths and steadily improves it for a crack length of 18.67 mm. An interpretation of the Williams results is that at a crack length of 18.67 mm the crack tip stress field is not being characterised as well by the single parameter approximation as with the higher order approximations. Again, in contrast, to this the CJP model remains the closest to the experimental data, supporting the earlier assertion that it is a wider-range elastic approximation to crack tip fields in the presence of plasticity-induced shielding than the Williams model.

Fig. 5 depicts the relative errors for the two crack tip stress models as a function of the experimental plastic zone area. The data clearly indicates the trends described above for the 1, 3 and 5-parameter Williams approximations and the CJP model.

Table 3 Experimental and estimated plastic zone area and corresponding relative error

| | | Experimental | CJP | Williams model | | |
				1st-term	3-terms	5-terms
Fig. 4a	Area (mm²)	0.8681	0.8549	0.8851	0.7746	0.7969
	e (%)	--	-1.52	1.96	-10.77	-8.20
Fig. 4b	Area(mm²)	1.2331	1.2853	1.3383	1.1157	1.1539
	e (%)	--	4.23	8.53	-9.52	-6.42
Fig. 4c	Area(mm²)	2.3750	2.5170	2.9684	2.0210	2.1420
	e (%)	--	5.98	24.98	-14.91	-9.81
Fig. 4d	Area(mm²)	3.4350	3.6072	4.5614	2.4240	2.5182

	e (%)	--	5.01	32.79	-29.43	-26.69
Fig. 4e	Area(mm²)	1.3554	1.3772	1.4995	1.1299	1.1721
	e (%)	--	1.61	10.63	-16.64	-13.52
Fig. 4f	Area(mm²)	0.4873	0.4593	0.4634	0.4401	0.4471
	e (%)	--	-5.75	-4.91	-9.69	-8.19

It should be noted that there are inevitably errors in the process of measuring and modelling the plastic zone. These include noise in the DIC measurements which would be amplified when calculating the strain field from the displacement field. Although the method presented in reference [28] is used to reduce the influence of noise on the calculated strain field, this error cannot be completely eliminated. Some studies have shown that the grain size of the material has a significant impact on the strain distribution at the crack tip and on the cumulative plastic strain distribution in the wake area [30]. At the same time, the passivation of the crack tip also has a certain effect on the plastic zone [32]. In addition, the numerical method used in this study to calculate the area of the plastic zone also contains errors. Quantifying these errors is complex but their magnitudes are likely to be consistent in all the modelling and the trends observed in plastic zone size calculation are expected to be correct.

Reference [33] describes the relationship between the crack tip plastic zone size and the stress-intensity factor, for the case of elastic-perfectly plasticity (EPP) with stress relaxation. As metallic alloys show non-ideal plastic deformation, this relationship can only be used as a reference, and the change in size of the theoretical plastic zone with stress-intensity factor does not accurately represent the change in the area of the plastic zone that arises from the stress redistribution attendant on plastic deformation. To a first approximation, the area of the plastic zone can be estimated by recording the number of DIC measurement points inside the plastic zone and comparing this with the total number of measurement points in the DIC region. From this, the area of the crack tip plastic zone can be estimated at any value of applied load. Fig. 6 gives typical results from this calculation for a crack length of 18.27 mm, with a quadratic relationship between plastic zone area and load that reflects the power law relationship in the definition of the Irwin stress intensity factor and the plastic zone size.

In the CJP model, K_F is the stress intensity factor that drives crack growth and it can be calculated as a function of load using the same nonlinear algorithm as done previously. As shown in Fig. 7 a linear relationship can then be obtained between K_F and plastic zone size, the linear correlation coefficient of

which is 0.9859.   This indicates that K_F is a direct measure of the driving force for crack growth.

In terms of the CJP model, the effective stress-intensity factor that ultimately drives crack propagation is calculated using the following formula [19]:

$$\Delta K_{CJP} = K_{\max,CJP} - K_{\min,CJP} = \Delta K_F - \Delta K_R$$

Fig. 8 shows a comparison between the values of $K_{\max,CJP}$ and K_I at peak load during crack propagation as a function of crack length. The magnitude of $K_{\max,CJP}$ is larger at crack lengths approximately < 17.5 mm, and then it decreases below the Irwin value. This is interpreted as reflecting the influence of the shielding effect of the additional stresses that are included in the CJP model, i.e. a distribution of wake contact stress behind the crack tip and the compatibility stresses induced at the elastic–plastic boundary. In the early stages of crack propagation the contribution from the shielding stresses reduces the effective applied stress intensity through the contribution from K_R, while at larger crack lengths crack blunting reduces the value of $K_{\max,CJP}$ below that of the Irwin stress intensity value. This blunting influence is the reason why the CJP formulation of stress intensity range rationalises crack growth data over a wider range of growth rates than the traditional value of ΔK. Fig. 9 plots the relationship between ΔK_I and ΔK_{CJP} and then fits this relationship with linear and cubic functions. The fit provided by the cubic function is very close for the DENT geometry, although a linear function could be used in engineering applications, noting that fitting line does not have a 45° slope.

5 Conclusion

The conclusions that can be drawn from this work are summarised below.

(1) This paper has proposed a calculation method based on the L-M nonlinear iterative algorithm to solve for the parameters of the CJP model. Based on an error analysis of the first term in the Williams crack tip stress equation and a generalization of the Saint-Venant principle, a suitable fitting area is selected to solve for the CJP model parameters. A comparative analysis between the experimentally measured and theoretically calculated plastic zones shows that the algorithm is effective and that the proposed selection method for the fitting zone is accurate.

(2) At all crack lengths considered, the CJP model provides the closest estimate of the crack tip plastic zone with relative errors, e, ranging from -1.52% at a crack length of 17.26 mm to +5.98% at 18.77 mm. In contrast, errors for the first term approximation of the Williams model ranges from +1.96% (17.26 mm) to +24.98% (18.27 mm). These relative errors decrease again for both the CJP and Williams models at a crack length of 18.67 mm.

(3) Using a three or five term Williams approximation decreases the accuracy of the fit at the three smaller crack lengths and improves it for a crack length of 18.67 mm. An interpretation of the Williams results is that at a crack length of 18.67 mm the crack tip stress field is not being characterised as well by the single parameter approximation as with the higher order approximations.

(4) Comparing the values of $K_{\max,CJP}$ and K_I at peak load during crack propagation, as a function of crack length, shows that the magnitude of $K_{\max,CJP}$ is larger at crack lengths approximately < 17.5 mm, and then it decreases below the Irwin value. This is interpreted as reflecting the influence of the shielding effect of the additional stresses that are included in the CJP model, i.e. a distribution of wake contact stress behind the crack tip and the compatibility stresses induced at the elastic–plastic boundary. In the early stages of crack propagation the contribution from the shielding stresses reduces the effective applied stress intensity through the contribution from K_R, while at larger crack lengths crack blunting reduces the value of $K_{\max,CJP}$ below that of the Irwin stress intensity value. This blunting influence is the reason why the CJP formulation of stress intensity range rationalises crack growth data over a wider range of growth rates than the traditional value of ΔK.

(5) There is a linear relationship with a linear correlation coefficient of 0.9859 between the stress-intensity factor, K_F, and the area of the plastic zone at the crack tip, indicating that the CJP model is providing a good descriptor for fatigue crack growth rate in the presence of shielding.
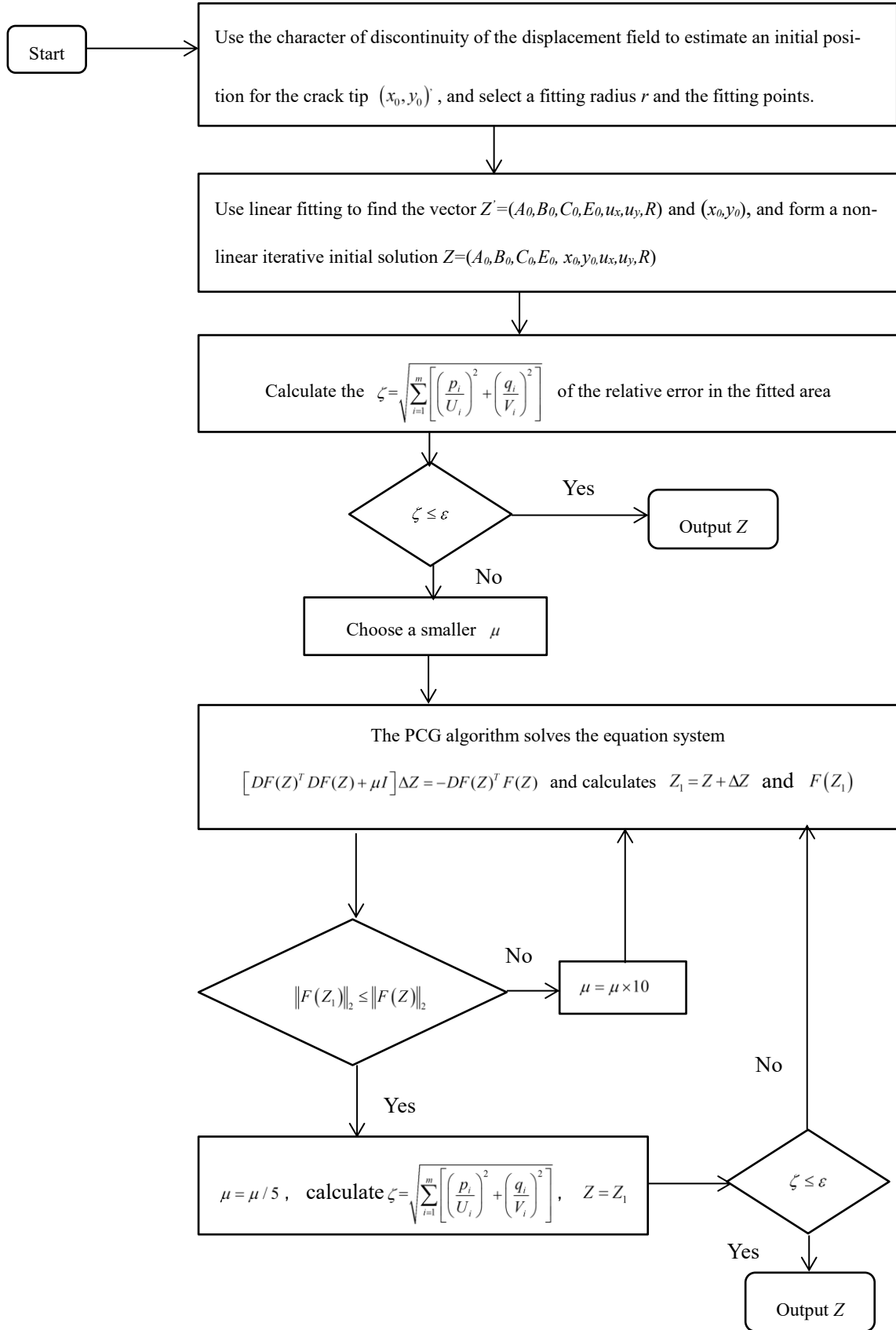
Acknowledges

his assistance in the work.

References

[1]. Rice JR, Mechanics of crack tip deformation and extension by fatigue. Fatigue Crack Propagation, ASTM STP 415, (1967), 247-311.

[2]. Elber W. The Significance of Fatigue Crack Closure [J]. Damage Tolerance in Aircraft Structures, ASTM International, 1971: 230-242..

[3]. Willenborg J., Engle R.M., Wood H.A. A crack growth retardation model using an effective stress concept. Technical Memorandum 71-1-FBR, (1971), Air Force Flight Dynamics Laboratory, Wright-Patterson Air Force Base.

[4]. Newman Jr J C. A Finite-Element Analysis of Fatigue Crack Closure. ASTM STP 590, (1976), 281-301

[5]. Newman Jr J C. A crack opening stress equation for fatigue crack growth. International Journal of Fracture, (1984), 24:R131–R135.

[6]. Kujawski D. A new $(\Delta K+K_{max})^{0.5}$ driving force parameter for crack growth in aluminum alloys. International Journal of Fatigue, (2001), 23(8):733-740.

[7]. Huang XP, Torgeir Moan. Improved modeling of the effect of R -ratio on crack growth rate. International Journal of Fatigue, (2006), 29:591-602.

[8]. Beevers CJ, Bell K, Carlson RL and Starke EA. A model for fatigue crack closure. Engineering Fracture Mechanics, (1984), 19(1):93-100.

[9]. Vasco-Olmo JM, Díaz FA, James MN and Bing Yang. Crack tip plastic zone evolution during an overload cycle and the contribution of plasticity-induced shielding to crack growth rate changes. Fatigue and Fracture of Engineering Materials and Structures, (2018) 41:2172-2186.

[10]. Pacey MN, James MN, Patterson EA. A New Photoelastic Model for Studying Fatigue Crack Closure. Experimental Mechanics, 2005, 45(1):42-52.

[11]. Christopher CJ, James MN, Patterson EA, et al. Towards a new model of crack tip stress fields. International Journal of Fracture, 2007; 148(4):361-371.

[12]. James MN, Christopher CJ, Yanwei Lu and Patterson EA. Local crack plasticity and its influences on the global elastic stress field. International Journal of Fatigue; 2013; 46:4-15.

[13]. Vasco-Olmo JM, James MN, Christopher CJ, Patterson EA and Díaz FA. Assessment of crack tip

plastic zone size and shape and its influence on crack tip shielding. Fatigue & Fracture of Engineering Materials & Structures 2016; 39(8): 969-981.

[14]. Yoneyama S, Ogawa T, Kobayashi Y. Evaluating mixed-mode stress intensity factors from full-field displacement fields obtained by optical methods. ENGINEERING FRACTURE MECHANICS; 2007; 74: 1399-1412.

[15]. Yoneyama S, Morimoto Y, Takashi M. Automatic Evaluation of Mixed-mode Stress Intensity Factors Utilizing Digital Image Correlation. Strain; 2006; 42(1):21-29.

[16]. Yoneyama S, Kobayashi Y, Ogawa T. 604 A Method for Evaluating Mixed-mode Stress Intensity Factors from Displacement Fields around a Crack Tip[J]. Transactions of the Japan Society of Mechanical Engineers Series A, 2006, 72(719):1025-1032.

[17]. Chernyatin AS, Lopez-Crespo P, Moreno B, et al. Multi-approach study of crack-tip mechanics on aluminium 2024 alloy. Theoretical and Applied Fracture Mechanics; 2018; 98:38-47.

[18]. Zanganeh M, Lopez-Crespo P, Tai YH, et al. Locating the Crack Tip Using Displacement Field Data: A Comparative Study. Strain; 2013; 49(2):102-115.

[19]. Bing Yang, Vasco-Olmo JM, Díaz FA and James MN, A more effective rationalisation of fatigue crack growth rate data for various specimen geometries and stress ratios using the CJP model. International Journal of Fatigue 2018; 114:189-197.

[20]. Williams ML. On the Stress Distribution at the Base of a Stationary Crack. Journal of Applied Mechanics 1957; 24(1):109-114.

[21]. Muskhelishvili N.I. Some Basic Problems of the Mathematical Theory of Elasticity. Noordhoff International Publishing, Groningen, Holland, 1977.

[22]. Liang DC. Hybrid experimental and numerical investigation on the fracture behavior and toughening mechanism of short plant fiber reinforced composites. PhD thesis, Tianjin University 2013. (in Chinese).

[23]. Christopher CJ, Laboviciute G, James MN and Patterson EA. Extension of the CJP model to mixed mode I and mode II. Frattura ed Integrità Strutturale 2013; 25: 161-166.

[24]. Wang DR. Nonlinear equations solution and optimal method. People's Education Press; Beijing 1979:244-260 (in Chinese).

[25].   Zhou RZ and Liu GT. On the truncation error of the main term in the expansion of Williams complex characteristics. Journal of Fuzhou University (Natural Science Edition) 1986; (02): 89-100 (in Chinese).

[26].   Xu ZL. A concise course in elasticity, Fourth Edition. Higher Education Press; Beijing 2013:37-38 (in Chinese).

[27]. Suzuki H, Mcevily A J . Microstructural effects on fatigue crack growth in a low carbon steel. Metallurgical Transactions A, 1979; 10(4):475-481.

[28]. Pan B, Xie HM, Guo ZQ, Hua T. Full-field strain measurement using a two-dimensional Savitzky-Golay digital differentiator in digital image correlation. Optical Engineering. 2007; 46(3): 033601.

[29]. Vasco-Olmo JM, Diaz FA, James MN, et al. Crack tip plastic zone evolution during an overload cycle and the contribution of plasticity-induced shielding to crack growth rate changes [J]. Fatigue & Fracture of Engineering Materials & Structures 2018; 41(10): 2172-2186.

[30]. Ahadi A， Sun Q. Grain size dependence of fracture toughness and crack-growth resistance of superelastic NiTi. Scripta Materialia. 2016; 113: 171-175.

[31]. Carroll J D , Abuzaid W , Lambros J , et al. High resolution digital image correlation measurements of strain accumulation in fatigue crack growth. International Journal of Fatigue. 2013; 57:140-150.

[32]. Zhang W, Liu Y. Plastic zone size estimation under cyclic loadings using in situ optical microscopy fatigue testing. Fatigue & Fracture of Engineering Materials & Structures. 2011; 34(9):717-727.

[33]. Irwin G R . Plastic zone near a crack and fracture toughness. In: Proceedings of the 7th Sagamore Research Conference on Mechanics & Metals Behavior of Sheet Material. New York, 1960, 4:463-478.
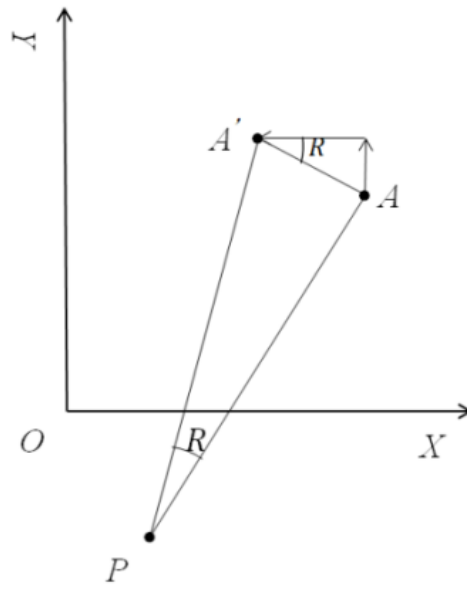
Flowchart 1: Non-linear iterative algorithm

Start

Use the character of discontinuity of the displacement field to estimate an initial position for the crack tip $(x_0, y_0)'$, and select a fitting radius r and the fitting points.

Use linear fitting to find the vector $Z'=(A_0,B_0,C_0,E_0,u_x,u_y,R)$ and (x_0,y_0), and form a non-linear iterative initial solution $Z=(A_0,B_0,C_0,E_0,\ x_0,y_0,u_x,u_y,R)$

Calculate the $\zeta = \sqrt{\sum_{i=1}^{m}\left[\left(\dfrac{p_i}{U_i}\right)^2 + \left(\dfrac{q_i}{V_i}\right)^2\right]}$ of the relative error in the fitted area

$\zeta \le \varepsilon$

Yes

Output Z

No

Choose a smaller μ

The PCG algorithm solves the equation system

$\left[DF(Z)^T DF(Z) + \mu I\right]\Delta Z = -DF(Z)^T F(Z)$ and calculates $Z_1 = Z + \Delta Z$ and $F(Z_1)$

$\left\|F(Z_1)\right\|_2 \le \left\|F(Z)\right\|_2$

No

$\mu = \mu \times 10$

Yes

$\mu = \mu / 5$, calculate $\zeta = \sqrt{\sum_{i=1}^{m}\left[\left(\dfrac{p_i}{U_i}\right)^2 + \left(\dfrac{q_i}{V_i}\right)^2\right]}$, $Z = Z_1$

$\zeta \le \varepsilon$

No

Yes

Output Z

Fig. 1 Schematic diagram of small rotation
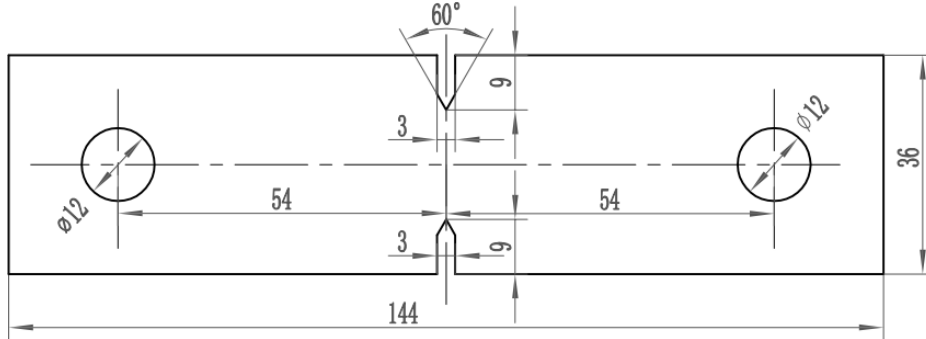
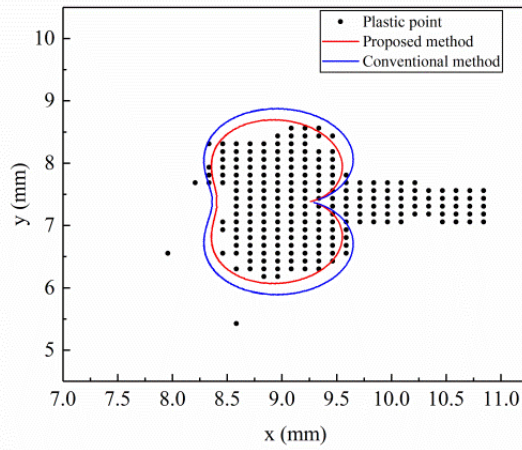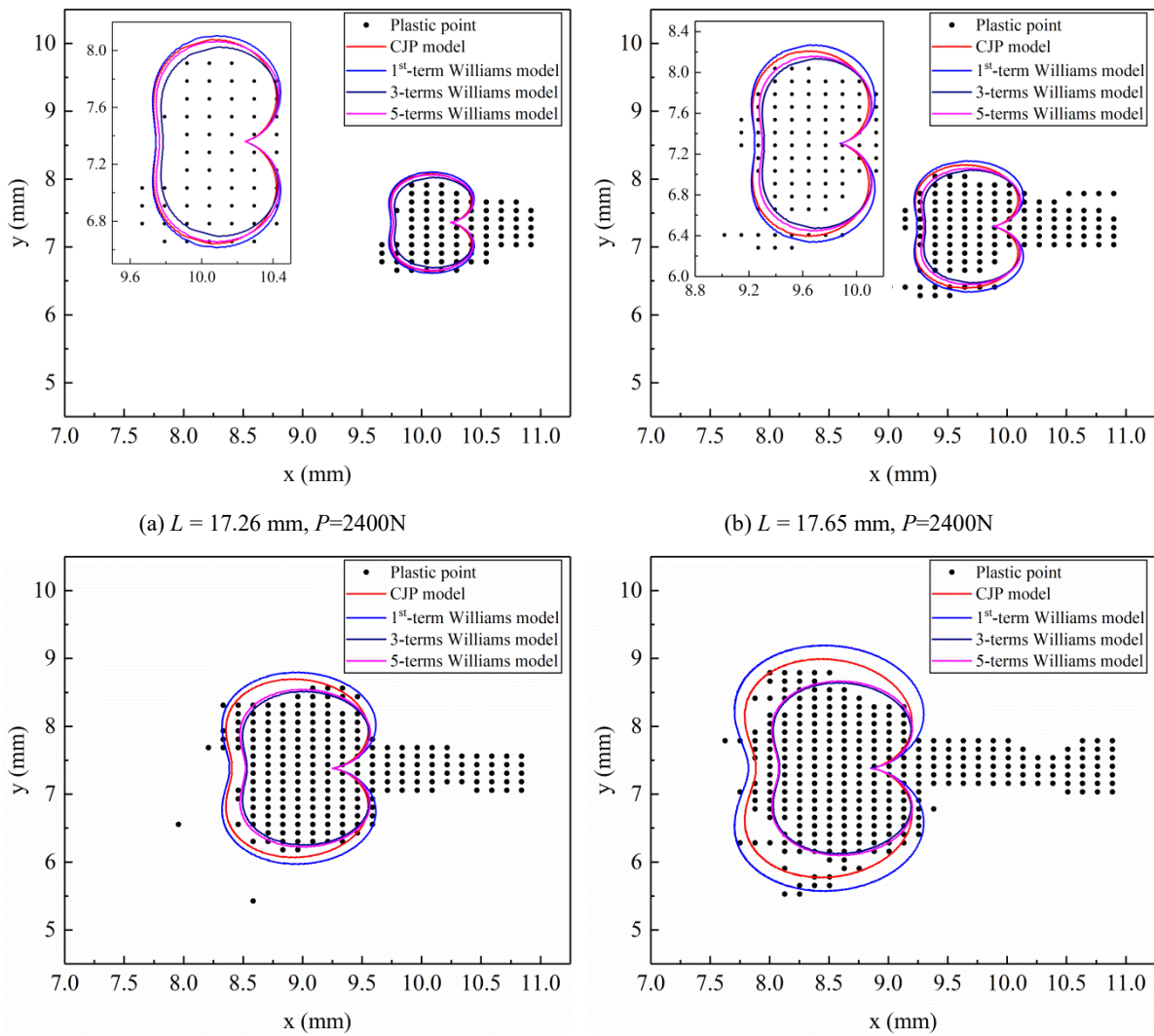**Fig. 2** Dimensions of the double edge-notched specimen

Fig. 3 The plastic zones indicated by the CJP model before (conventional) and after (proposed) optimisation of the

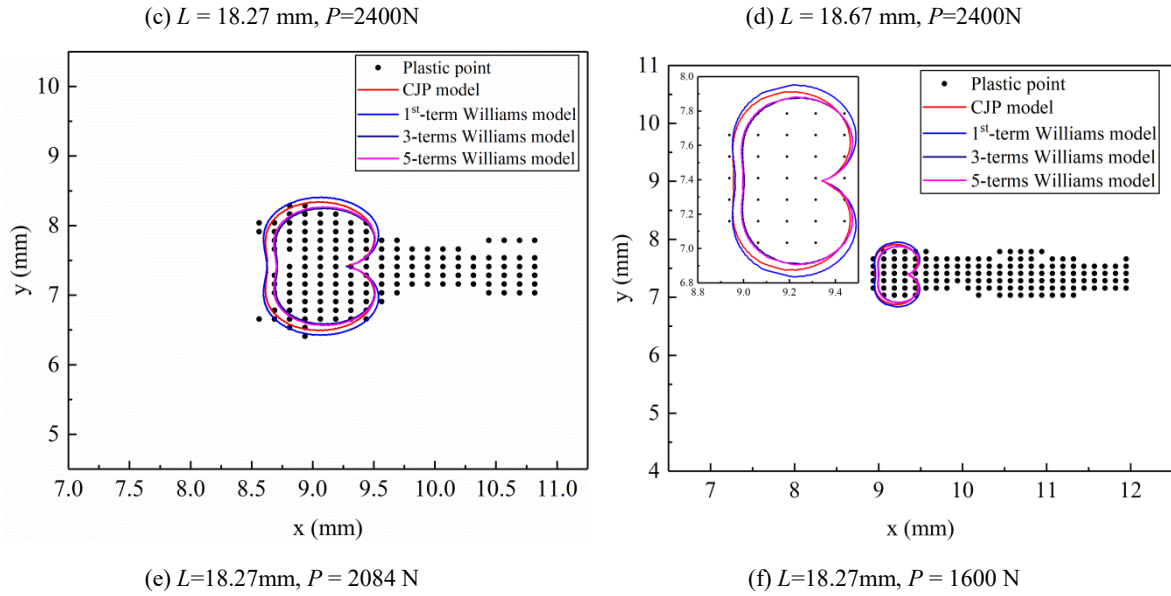crack tip position, compared with the experimentally determined plastic zone

(a) L = 17.26 mm, P=2400N

(b) L = 17.65 mm, P=2400N

(c) *L* = 18.27 mm, *P*=2400N   (d) *L* = 18.67 mm, *P*=2400N

(e) *L*=18.27mm, *P* = 2084 N   (f) *L*=18.27mm, *P* = 1600 N

Fig. 4 Comparison between the experimental plastic zone size and the predictions obtained using different models
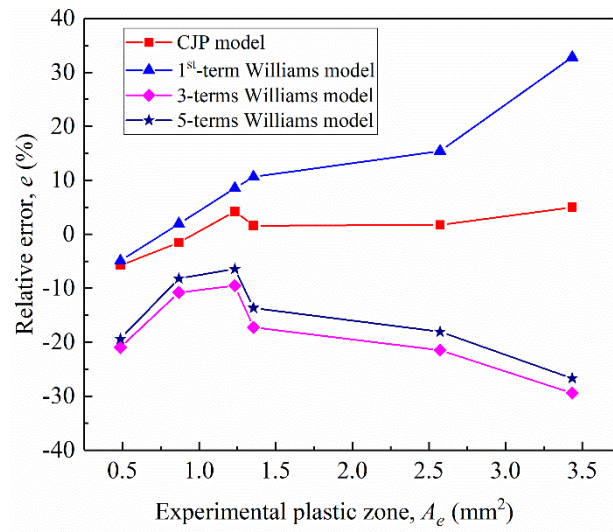
Fig. 5 Relationship between the relative error and the experimental plastic zone areas
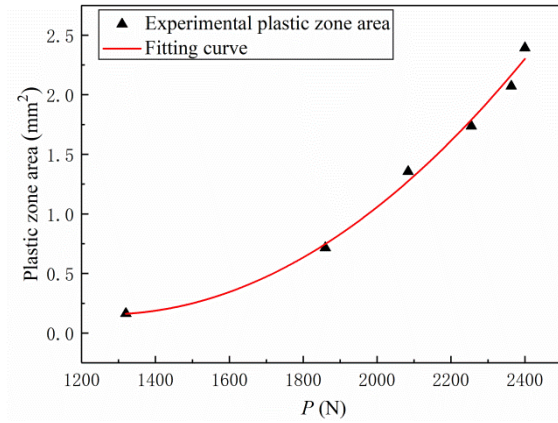
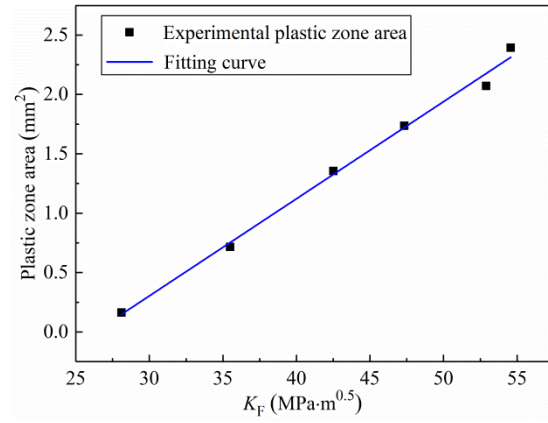**Fig. 6** Relationship between plastic zone area and load for

a crack length of 18.27 mm

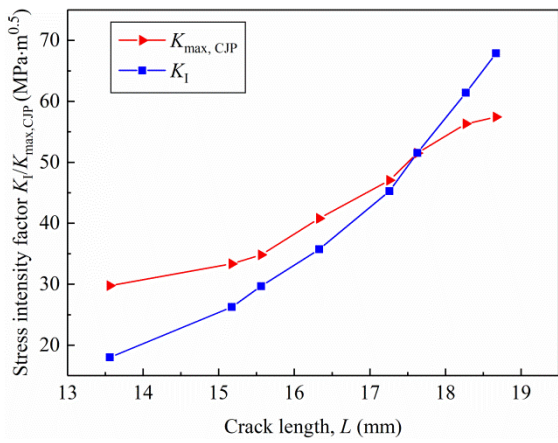**Fig. 7** Relationship between plastic zone area and K_F

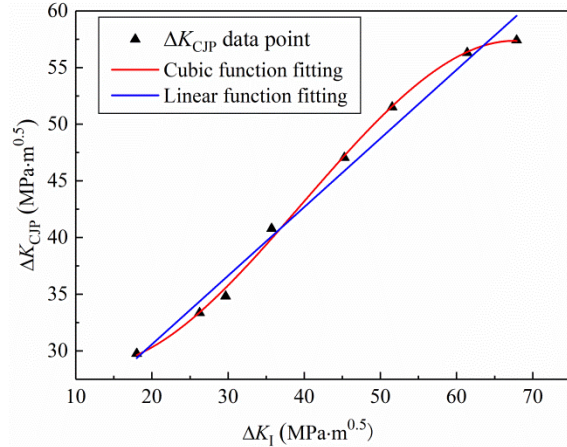**Fig. 8** Relationship between crack length and stress-in-

tensity factor

Fig. 9 ΔK_I and ΔK_{CJP} fitting curves